Thermophysical Properties of Mixtures of 2-Ethylhexanoic Acid and *p*-Xylene

Babette Kunstmann, Hans Hasse, and Maximilian Kohns*

RPTU Kaiserslautern

Laboratory of Engineering Thermodynamics (LTD)

Erwin-Schrödinger-Str. 44

67663 Kaiserslautern, Germany

E-mail: maximilian.kohns@rptu.de

Abstract

In this work, the density, viscosity, thermal conductivity, and isobaric heat capacity of mixtures of 2-ethylhexanoic acid (EHA) and *p*-xylene, as well as self-diffusion coefficients of both components were measured at 101.3 kPa and temperatures between 293.15 and 353.15 K. Furthermore, vapor-liquid equilibria of this system were studied at 10 and 20 kPa. Parameters for correlations of all properties are reported together with the data in this work to facilitate the application of the results in modeling and simulation of spray flame synthesis.

Introduction

2-Ethylhexanoic acid (EHA) and xylene are commonly used solvents in spray flame synthesis of nanoparticles. Mixtures of these components are suitable solvents for various precursors.[1–7] Moreover, when studying spray flame processes with numerical techniques, mixtures of EHA and xylene can be used as a simpler, surrogate model system for the frequently used precursor solutions containing metal 2-ethylhexanoates and xylene.[8–11] In the mentioned applications, all three isomers of xylene, i.e., *o*-xylene, *m*-xylene, and *p*-xylene, occur. However, the influence of the choice of the isomer on the overall spray flame process is expected to be marginal. The *p*-xylene isomer is studied in this work to maintain consistence with previous work.[12]

Despite their relevance especially in the field of spray flame synthesis, to the best of our knowledge, no data on the properties of mixtures of EHA and xylene are available in the literature. Due to its use as an industrial solvent and intermediate,[13] data on the properties of pure *p*-xylene are sufficiently available. The properties of pure EHA were extensively studied in our previous work on mixtures of EHA and ethanol.[14]

In this work, the density, the viscosity, the thermal conductivity, and the isobaric heat capacity of mixtures of EHA and *p*-xylene, as well as the self-diffusion coefficients of both components were measured at temperatures between 293.15 K and 353.15 K and atmospheric pressure over the entire composition range. Additionally, vapor-liquid equilibria (VLE) were investigated at 10 kPa and 20 kPa.

Experimental

Chemicals and Sample Preparation

Table 1 lists the CAS registry numbers, suppliers, and purities of the chemicals used in this work.

Table 1: Chemicals

	CAS reg. no.	supplier	mole fraction purity[a]
2-ethylhexanoic acid (EHA)	149-57-5	Sigma-Aldrich	0.998
p-xylene	106-42-3	Thermo Fischer Scientific	0.997
1,4-dioxane	123-91-1	Sigma-Aldrich	0.9993

[a] As specified by supplier

Small samples (sample mass < 50 g) were needed for the self-diffusion coefficient measurements and were prepared gravimetrically using a Mettler-Toledo laboratory balance (specified standard uncertainty $u(m) = 0.0001$ g). Larger samples were needed for the density and viscosity measurements as well as the thermal conductivity and isobaric heat capacity measurements and were prepared using a Mettler-Toledo PR2003 Comparator laboratory balance (specified standard uncertainty $u(m) = 0.001$ g). The combined expanded uncertainty of the composition of the samples is $U(x_{\mathrm{Xyl}}) = 0.001$ mol mol^{-1} ($k = 2$).

For the VLE measurements, about 100 – 200 ml of feed mixture were needed for each run. The equilibrium compositions of the vapor and liquid phase depend on the temperature, the pressure, and the local composition in the apparatus. Therefore, their dependence on the feed composition is fuzzy and, for simplicity, the feed for the VLE measurements was prepared volumetrically.

Measurements

The measurement methods for the density, viscosity, thermal conductivity, isobaric heat capacity, and self-diffusion coefficients were the same as in our previous work.[12,14–16] In

these references and their supporting information documents, validations of the measurement results for pure *p*-xylene[12] and for pure EHA[14] were provided for all investigated thermophysical properties. We hence refrain from repeating these validations here.

Density and Viscosity

The density and viscosity were measured using a combined instrument (SVM 3000, Anton Paar), comprising a vibrating-u-tube densimeter and a rotational viscosimeter. The combined expanded uncertainty of the density measurement was $U(\rho) = 1$ kg m^{-3} ($k = 2$), the relative combined expanded uncertainty for the viscosity was $U_{\mathrm{rel}}(\eta) = 0.02$ ($k = 2$), and the standard uncertainty of the temperature measurement specified by the manufacturer was $u(T) = 0.05$ K.

Thermal Conductivity and Isobaric Heat Capacity

The thermal conductivity and the thermal diffusivity were measured using a transient hot-wire thermal conductivity meter (LAMBDA, flucon fluid control GmbH). The isobaric heat capacity was then calculated from the thermal conductivity λ, the thermal diffusivity a, and the (previously measured) density ρ:

$$c_p = \frac{\lambda}{a\ \rho} \tag{1}$$

The combined expanded relative uncertainties were $U_{\mathrm{rel}}(\lambda) = 0.04$ ($k = 2$) for the thermal conductivity measurement and $U_{\mathrm{rel}}(c_p) = 0.06$ ($k = 2$) for the isobaric heat capacity, and the standard uncertainty of the temperature measurement was estimated to be $u(T) = 0.1$ K.

Self-Diffusion Coefficients

The self-diffusion coefficients were measured using pulsed field gradient (PFG) ^{1}H NMR spectroscopy. The NMR spectrometer consisted of an Ascend 400 magnet and an Avance III HD 400 console (Bruker). The measurements were carried out as described in Refs. 17 and 18. The self-diffusion coefficients were obtained from a fit to the Stejskal-Tanner equation.[19] The

standard uncertainty of the temperature measurement was estimated to be $u(T) = 0.1$ K. The combined expanded relative uncertainty of the self-diffusion coefficient measurement is typically about $U_{\mathrm{rel}}(D) = 0.01$ ($k = 2$) but can be higher depending on composition and temperature. It was therefore stated explicitly for each individual experimental data point.

Vapor-Liquid Equilibrium

The VLE were measured with a co-current thin-film evaporator as described in Refs. 20–22. The pressure was measured using a pressure sensor of type VSR53DL by Thyracont and the temperature was measured using a Pt100 resistance thermometer which was calibrated against a standard certified by Physikalisch-Technische Bundesanstalt (PTB, Braunschweig, Germany). The standard uncertainties of the temperature and pressure measurements are $u(T) = 0.1$ K and $u(p) = 0.1$ kPa, respectively. As in our previous work,[14] the compositions of the samples taken from the liquid and the vapor phase were analyzed by gas chromatography (GC). The GC system (Agilent 7890A) was equipped with a flame ionization detector (FID) and a Zebron Phenomenex ZB-FFAP (30 m x 0.32 mm x 0.5 µm) column. 1,4-Dioxane was employed as an internal standard. From analyzing gravimetrically prepared samples, the standard uncertainty of the *p*-xylene mole fraction was estimated to be $u(x_{\mathrm{Xyl}}) = u(y_{\mathrm{Xyl}}) = 0.01$ mol mol^{-1}.

Modeling

Density, Thermal Conductivity and Isobaric Heat Capacity

The density, thermal conductivity, and isobaric heat capacity were correlated using polynomials for the description of the temperature dependence of the pure component properties and Redlich-Kister polynomials for the description of the mixture properties. The modeling approach was the same as in our previous work.[12,14,23]

The modeling approach is described here using the exemplary property z. The mixture property z was written as a function of the pure component properties z_i^{pure}, the mole fractions of the components x_i, and an excess term z^{E}.

$$z = x_{\text{EHA}} z_{\text{EHA}}^{\text{pure}} + x_{\text{Xyl}} z_{\text{Xyl}}^{\text{pure}} + z^{\text{E}} \tag{2}$$

The pure component properties z_i^{pure} were calculated from a polynomial with the adjustable parameters a_i, b_i, and c_i.

$$z_i^{\text{pure}}/[z] = a_i + b_i \; T/\text{K} + c_i \; (T/\text{K})^2 \tag{3}$$

Here, $[z]$ is the unit of z, so that the adjustable parameters are dimensionless. The excess term z^{E} was calculated using a Redlich-Kister-type polynomial with the adjustable parameters E, F, and G.

$$z^{\text{E}}/[z] = (E + F \; T/\text{K} + G x_{\text{EHA}} x_{\text{Xyl}}) \; x_{\text{EHA}} x_{\text{Xyl}} \tag{4}$$

For convenience, we modeled the molar volume v instead of the specific density ρ. These quantities are related by:

$$v = \frac{\bar{M}}{\rho}, \tag{5}$$

where $\bar{M}$ is the average molar mass that was calculated from the molar masses of EHA

(M_{EHA}) and *p*-xylene (M_{Xyl}):

$$\bar{M} = x_{\mathrm{EHA}} M_{\mathrm{EHA}} + x_{\mathrm{Xyl}} M_{\mathrm{Xyl}}. \tag{6}$$

Viscosity

As in previous work,[12,23] the Jouyban-Acree correlation[24] was used to correlate the mixture viscosity:

$$\begin{aligned} \ln\left(\eta \ / \ \mathrm{mPa\ s}\right) =& x_{\mathrm{EHA}} \ln\left(\eta_{\mathrm{EHA}}^{\mathrm{pure}} \ / \ \mathrm{mPa\ s}\right) + x_{\mathrm{Xyl}} \ln\left(\eta_{\mathrm{Xyl}}^{\mathrm{pure}} \ / \ \mathrm{mPa\ s}\right) + E^{(\eta)} \left(\frac{x_{\mathrm{EHA}} x_{\mathrm{Xyl}}}{T/\mathrm{K}}\right) \\ &+ F^{(\eta)} \left(\frac{x_{\mathrm{EHA}} x_{\mathrm{Xyl}} (x_{\mathrm{Xyl}} - x_{\mathrm{EHA}})}{T/\mathrm{K}}\right) + G^{(\eta)} \left(\frac{x_{\mathrm{EHA}} x_{\mathrm{Xyl}} (x_{\mathrm{Xyl}} - x_{\mathrm{EHA}})^2}{T/\mathrm{K}}\right) \end{aligned} \tag{7}$$

The temperature dependence of the pure component viscosity η_i^{pure} was described by an exponential function with the adjustable parameters $a_i^{(\eta)}$, $b_i^{(\eta)}$, and $c_i^{(\eta)}$.

$$\eta_i^{\mathrm{pure}} \ / \ \mathrm{mPa\ s} = a_i^{(\eta)} \exp\left(\frac{b_i^{(\eta)}}{T/\mathrm{K}}\right) + c_i^{(\eta)} \tag{8}$$

Self-Diffusion Coefficients

The self-diffusion coefficients D_i were described by a polynomial function of temperature and composition, i.e., the *p*-xylene mole fraction x_{Xyl}, see Eq. (9). A similar correlation was previously used in our previous work on mixtures of EHA and ethanol,[14] which had been adapted from the correlation established in our previous work on mixtures of titanium(IV) isopropoxide (TTIP) and *p*-xylene.[12]

$$D_i \ / \ (10^{-9}\ \mathrm{m^2\ s^{-1}}) = a_i + b_i\ T/\mathrm{K} + (c_i + d_i\ T/\mathrm{K})\ x_{\mathrm{Xyl}} + (e_i + f_i\ T/\mathrm{K})\ x_{\mathrm{Xyl}}^3 \tag{9}$$

Therein, a_i - f_i are adjustable parameters.

Vapor-Liquid Equilibrium

The VLE were modeled based on the extended Raoult's law assuming the gas phase to be ideal and neglecting the pressure dependence of the chemical potential in the liquid phase:

$$p_i^{\mathrm{s}}\, x_i\, \gamma_i = p\, y_i \tag{10}$$

Therein, p_i^{s} is the vapor pressure of the pure component i, x_i is the liquid phase mole fraction of component i, γ_i is the activity coefficient of component i, p is the pressure, and y_i is the gas phase mole fraction of component i. The pure component vapor pressures p_i^{s} were described by an Antoine-type equation:

$$\ln(p_i^{\mathrm{s}}\ /\ \mathrm{kPa}) = A_i + \frac{B_i}{T/\mathrm{K} + C_i} \tag{11}$$

The parameters A_i, B_i, and C_i were taken from Refs. 14 and 12, where they were obtained from a fit to literature data.[25,26] The activity coefficients γ_i were modeled using the non-random two-liquid (NRTL) model[27]:

$$\ln \gamma_i = x_j^2 \left[\tau_{ji} \left(\frac{G_{ji}}{x_i + x_j G_{ji}} \right)^2 + \frac{\tau_{ij} G_{ij}}{(x_j + x_i G_{ij})^2} \right], \tag{12}$$

where

$$G_{ij} = \exp\left(-\alpha \tau_{ij}\right). \tag{13}$$

The adjustable parameters of the NRTL model are the non-randomness parameter α and the binary interaction parameters τ_{ij}. The parameter α was set to 0.3 following the recommendations in the original publication of the model.[27]

Fitting Procedure

The *python* solvers *numpy.polyfit* and *scipy.optimize.curve_fit* were used to fit the adjustable parameters, using the sum of squared deviations between measured z_j^{exp} and calculated values z_j^{cal} as the objective function (OF):

$$\mathrm{OF}_z = \sum_{j=1}^{N} \left(z_j^{\mathrm{exp}} - z_j^{\mathrm{cal}} \right)^2 \tag{14}$$

Therein, N was the number of experimental data points measured for property z. For adjusting the binary interaction parameters $\tau_{\mathrm{EHA,Xyl}}$ and $\tau_{\mathrm{Xyl,EHA}}$ of the NRTL model to the VLE data, the objective used in Eq. (14) was the pressure p.

Results and Discussion

The experimental data for all measured properties were correlated as described in the previous section. In the following, the experimental data for the different studied properties are discussed together with the correlations. The parameters of the correlations for the pure component molar volumes, viscosities, thermal conductivities, and isobaric heat capacities of EHA and *p*-xylene are given in Table 2. The parameters of the correlations for the excess molar volumes, viscosities, thermal conductivities, and isobaric heat capacities of mixtures of EHA and *p*-xylene are given in Table 3. The parameters of the correlations for the self-diffusion coefficients of EHA and *p*-xylene in mixtures of EHA and *p*-xylene are given in Table 4.

The parameters of the Antoine-type equation used for the vapor pressures of pure EHA and pure *p*-xylene are repeated from Refs. 14 and 12 in Table 5. The parameters of the NRTL model for the calculation of the activity coefficients are given in Table 6.

Table 2: Parameters of the correlations for the pure-component properties of EHA[a] and *p*-xylene

Property	Eq.	a_i or $a_i^{(\eta)}$	b_i or $b_i^{(\eta)}$	c_i or $c_i^{(\eta)}$
$v_{\mathrm{EHA}}^{\mathrm{pure}}$ / m^3 mol^{-1}	(3)	1.1481×10^{-4}	1.5090×10^{-7}	0[b]
$\eta_{\mathrm{EHA}}^{\mathrm{pure}}$ / mPa s	(8)	7.4089×10^{-5}	3.3525×10^{3}	6.6045×10^{-1}
$\lambda_{\mathrm{EHA}}^{\mathrm{pure}}$ / W m^{-1} K^{-1}	(3)	1.0638×10^{-1}	3.4356×10^{-4}	-7.9010×10^{-7}
$c_{p,\mathrm{EHA}}^{\mathrm{pure}}$ / J mol^{-1} K^{-1}	(3)	1.2608×10^{2}	4.4382×10^{-1}	0[b]
$v_{\mathrm{Xyl}}^{\mathrm{pure}}$ / m^3 mol^{-1}	(3)	8.3752×10^{-5}	1.3460×10^{-7}	0[b]
$\eta_{\mathrm{Xyl}}^{\mathrm{pure}}$ / mPa s	(8)	4.2349×10^{-3}	1.4209×10^{3}	1.2468×10^{-1}
$\lambda_{\mathrm{Xyl}}^{\mathrm{pure}}$ / W m^{-1} K^{-1}	(3)	1.9795×10^{-1}	-2.1000×10^{-4}	-7.9645×10^{-8}
$c_{p,\mathrm{Xyl}}^{\mathrm{pure}}$ / J mol^{-1} K^{-1}	(3)	1.3144×10^{2}	1.8782×10^{-1}	0[b]

[a] Repeated from Ref. 14 for the reader's convenience
[b] Not needed and set to zero

Table 3: Parameters of the correlations for the excess properties of mixtures of EHA and *p*-xylene

Property	Eq.	E or $E^{(\eta)}$	F or $F^{(\eta)}$	G or $G^{(\eta)}$
v / m^3 mol^{-1}	(4)	-1.0615×10^{-6}	2.1219×10^{-9}	-9.2538×10^{-9}
η / mPa s	(7)	-1.9665×10^{2}	-2.5993×10^{1}	0[a]
λ / W m^{-1} K^{-1}	(4)	-5.0315×10^{-3}	2.4421×10^{-5}	-1.3071×10^{-3}
c_p / J mol^{-1} K^{-1}	(4)	-5.2968	1.4227×10^{-2}	-2.4412

[a] Not needed and set to zero

Table 4: Parameters of the correlations for the self-diffusion coefficients of EHA and *p*-xylene in mixtures of EHA and *p*-xylene (see Eq. (9))

Property	a_i	b_i	c_i	d_i	e_i	f_i
D_{EHA} / 10^{-9} m^2 s^{-1}	-2.026	7.191×10^{-3}	-1.974	8.290×10^{-3}	-5.905×10^{-1}	3.377×10^{-3}
D_{Xyl} / 10^{-9} m^2 s^{-1}	-3.560	1.289×10^{-2}	-4.861	2.131×10^{-2}	-7.765×10^{-2}	1.327×10^{-3}

Table 5: Antoine parameters for EHA and *p*-xylene obtained previously[12,14] from fits of Eq. (11) to the indicated literature data

Component	A	B	C	Ref.
EHA	15.2351	-4066.6	-117.614	25
p-xylene	14.0775	-3344.9	-57.910	26

Table 6: NRTL parameters obtained from a fit to the present experimental VLE data (see Eqs. (12) and (13))

α	$\tau_{\mathrm{EHA,Xyl}}$	$\tau_{\mathrm{Xyl,EHA}}$
0.3	-0.8640	2.3013

Density

Table 7 lists the experimental results for the density. They are shown in Figure 1 together with the correlation results. As expected, the density decreases with increasing temperature and increasing *p*-xylene mole fraction. While the density has a more complex dependence on the composition, the molar volume (see Appendix) exhibits an almost perfectly linear dependence on the *p*-xylene mole fraction, indicating an almost ideal mixing behavior.

Table 7: Results of the density measurements[a]

	ρ / kg m^{-3}				
	x_{Xyl} / mol mol^{-1}				
T / K	0[b]	0.25	0.5	0.75	1
293.15	906.4	897.4	887.4	875.2	861.1
303.15	898.2	889.1	879.0	866.6	852.4
313.15	890.0	880.9	870.5	858.0	843.5
323.15	882.0	872.6	862.0	849.4	834.9
333.15	873.8	864.3	853.5	840.7	826.0
343.15	865.7	856.0	844.9	831.9	817.1
353.15	857.6	847.6	836.3	823.2	808.1

[a] Density ρ, liquid mole fraction x_{Xyl}, and temperature T at $p = 101.3$ kPa. The combined expanded uncertainties are $U(\rho) = 1$ kg m^{-3} ($k = 2$), $U(x_{\mathrm{Xyl}}) = 0.001$ mol mol^{-1} ($k = 2$), $u(p) = 3$ kPa, and $u(T) = 0.05$ K.

[b] Repeated from Ref. 14 for the reader's convenience

Viscosity

Table 8 lists the experimental results for the viscosity. They are shown in Figure 2 together with the correlation results. Expectedly, the viscosity decreases strongly with increasing temperature and with increasing *p*-xylene mole fraction. In contrast to mixtures of EHA with ethanol, for which the viscosity surprisingly shows an almost linear dependence on the mole fraction,[14] the corresponding relation is strongly non-linear for mixtures of EHA and *p*-xylene. This is in line with our previous findings for mixtures of TTIP and *p*-xylene.[12]

Thermal Conductivity

Table 9 lists the experimental results for the thermal conductivity. They are shown in Figure 3 together with the correlation results. The thermal conductivity decreases with increasing temperature and decreasing *p*-xylene mole fraction. The difference between the

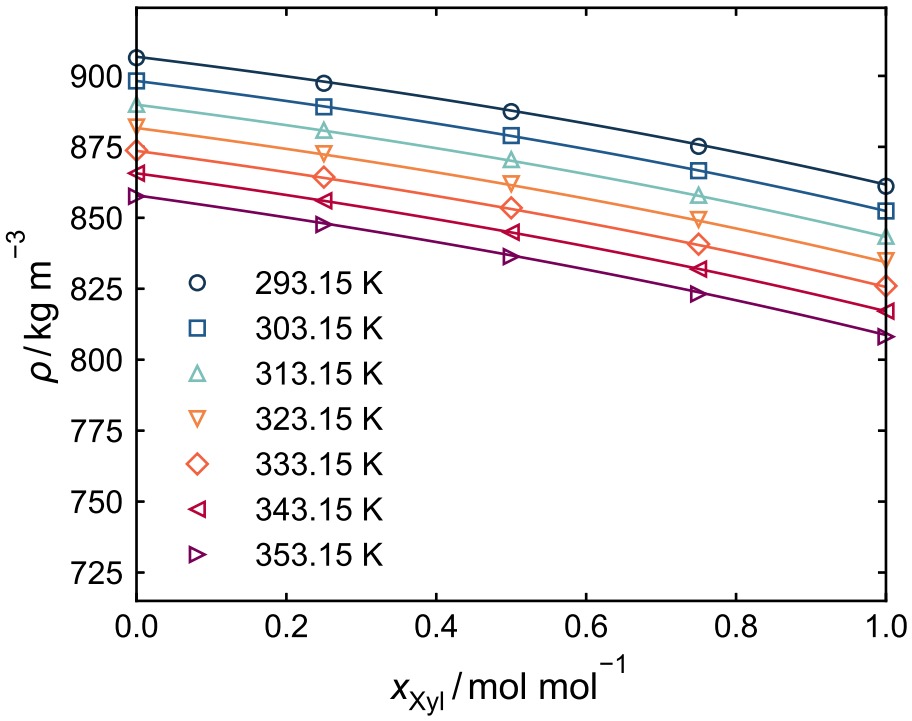

Figure 1: Density ρ of mixtures of EHA and p-xylene at 101.3 kPa and different temperatures. Symbols are experimental results. Experimental uncertainties are within symbol size. Lines are empirical correlations, cf. Eqs. (2) – (6), with parameters listed in Tables 2 and 3.

thermal conductivities of pure EHA and pure p-xylene is rather small, however, a clear deviation from linearity with respect to the composition and, thus, from ideal behavior is observed.

Isobaric Heat Capacity

Table 10 lists the experimental results for the isobaric heat capacity. They are shown in Figure 4 together with the correlation results. In agreement with expectations and previous results,[12,14] the isobaric heat capacity decreases almost perfectly linearly with increasing p-xylene mole fraction. Its temperature dependence is different to that of the other properties discussed so far: the isobaric heat capacity increases with increasing temperature.

Table 8: Results of the viscosity measurements[a]

	η / mPa s ($U(\eta)$ / mPa s)				
	x_{Xyl} / mol mol^{-1}				
T / K	0[b]	0.25	0.5	0.75	1
293.15	7.529 (0.146)	3.363 (0.031)	1.754 (0.015)	1.025 (0.010)	0.664 (0.006)
303.15	5.354 (0.046)	2.606 (0.024)	1.441 (0.021)	0.881 (0.008)	0.587 (0.005)
313.15	3.961 (0.034)	2.080 (0.018)	1.218 (0.011)	0.768 (0.008)	0.515 (0.009)
323.15	3.042 (0.026)	1.702 (0.015)	1.041 (0.009)	0.678 (0.006)	0.471 (0.005)
333.15	2.413 (0.021)	1.423 (0.013)	0.904 (0.008)	0.604 (0.006)	0.427 (0.004)
343.15	1.961 (0.017)	1.210 (0.011)	0.794 (0.007)	0.546 (0.008)	0.391 (0.004)
353.15	1.629 (0.014)	1.045 (0.009)	0.705 (0.006)	0.494 (0.005)	0.360 (0.004)

[a] Viscosity η, liquid mole fraction x_{Xyl}, and temperature T at $p = 101.3$ kPa. The combined expanded relative uncertainties of the viscosity $U(\eta)(k = 2)$ are given in the table and the other combined expanded uncertainties are $U(x_{\mathrm{Xyl}}) = 0.001$ mol mol^{-1} ($k = 2$), $u(p) = 3$ kPa, and $u(T) = 0.05$ K.

[b] Repeated from Ref. 14 for the reader's convenience

Self-Diffusion Coefficients

Table 11 and Table 12 list the experimental results for the self-diffusion coefficients of EHA and *p*-xylene, respectively. They are shown in Figure 5 together with the correlation results. EHA is a larger molecule than *p*-xylene. Therefore, as expected, the self-diffusion coefficient of EHA is always lower than that of *p*-xylene at the same temperature and composition. Both self-diffusion coefficients increase with increasing temperature and increasing *p*-xylene mole fraction.

Vapor-Liquid Equilibrium

Table 13 lists the results of the VLE measurements. They are shown in Figure 6 together with the model results. The VLE is wide-boiling and zeotropic. Although the NRTL model was only adapted to the pressure, the gas phase composition is also excellently reproduced.

At high *p*-xylene mole fractions, the activity coefficient of EHA (not shown) sharply

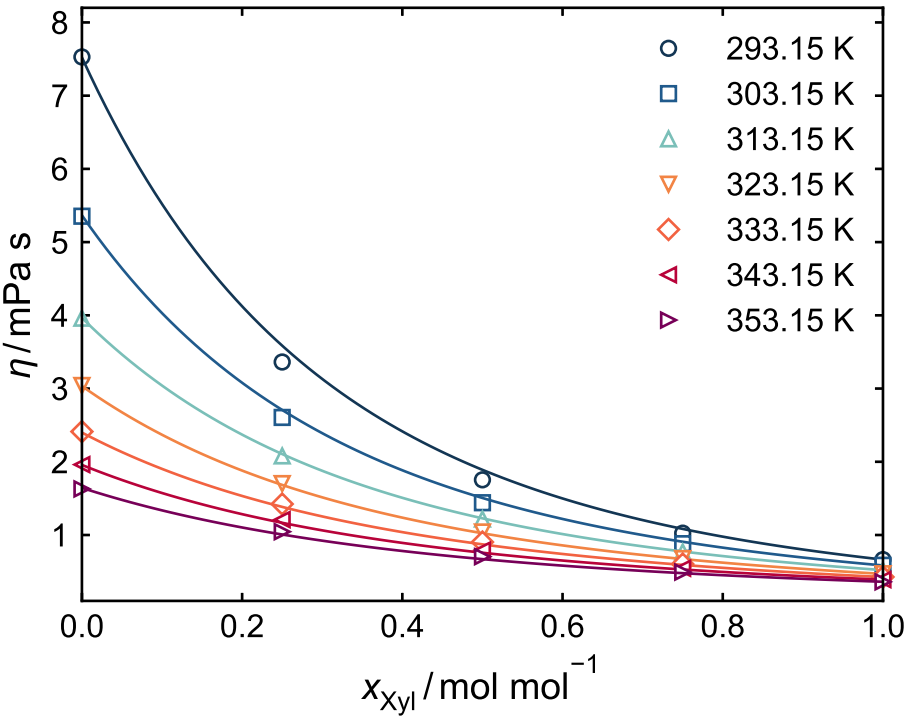

Figure 2: Viscosity η of mixtures of EHA and p-xylene at 101.3 kPa and different temperatures. Symbols are experimental results. Experimental uncertainties are within symbol size. Lines are empirical correlations, cf. Eqs. (7) and (8), with parameters listed in Tables 2 and 3.

increases and reaches high values. This is typical for an associating compound like EHA in a non-associating solvent like p-xylene.[28]

Lewis Number

When a droplet evaporates in a hot atmosphere, as is the case in spray flame synthesis, droplet explosions can occur. In Ref. 29, it was shown that this is caused by the fact that for mixtures typically used in such processes, heat transport is much faster than mass transport. The Lewis number Le is an important indicator for the ratio of heat and mass transport rates and, therefore, for the occurrence of superheating and droplet explosions.[30] For a binary mixture, Le is calculated from the thermal diffusivity a and the mutual Fickian diffusion

Table 9: Results of the thermal conductivity measurements[a]

	λ / W m^{-1} K^{-1}				
	x_{Xyl} / mol mol^{-1}				
T / K	0[b]	0.25	0.5	0.75	1
293.15	0.139	0.137	0.135	0.132	0.129
303.15	0.138	0.135	0.133	0.130	0.127
313.15	0.136	0.134	0.131	0.128	0.125
323.15	0.135	0.132	0.129	0.125	0.122
333.15	0.133	0.130	0.127	0.123	0.119
343.15	0.131	0.128	0.125	0.120	0.117
353.15	0.129	0.127	0.122	0.118	0.114

[a] Thermal conductivity λ, liquid mole fraction x_{Xyl}, and temperature T at $p = 101.3$ kPa. The combined expanded relative uncertainty of the thermal conductivity is $U_{\mathrm{rel}}(\lambda) = 0.04$ ($k = 2$) and the other combined expanded uncertainties are $U(x_{\mathrm{Xyl}}) = 0.001$ mol mol^{-1} ($k = 2$), $u(p) = 3$ kPa, and $u(T) = 0.1$ K.

[b] Repeated from Ref. 14 for the reader's convenience

coefficient D:

$$Le = \frac{a}{D} = \frac{\lambda}{\rho c_p D} \tag{15}$$

The property correlations from this work were used to calculate the Lewis number of mixtures of EHA and p-xylene. The thermal diffusivity was obtained using the correlations for the thermal conductivity, the density, and the isobaric heat capacity (see Eqs. (2) – (5) and Tables 2 and 3).

The correlation for the self-diffusion coefficients (see Eq. (9) and Table 4) were used for the extrapolation to infinite dilution. At infinite dilution, the self-diffusion coefficients become equal to the Maxwell-Stefan mutual diffusion coefficients $Đ^{\infty}_{\mathrm{EHA,Xyl}}$ and $Đ^{\infty}_{\mathrm{Xyl,EHA}}$. The Vignes correlation[31] was then used for calculating the Maxwell-Stefan mutual diffusion

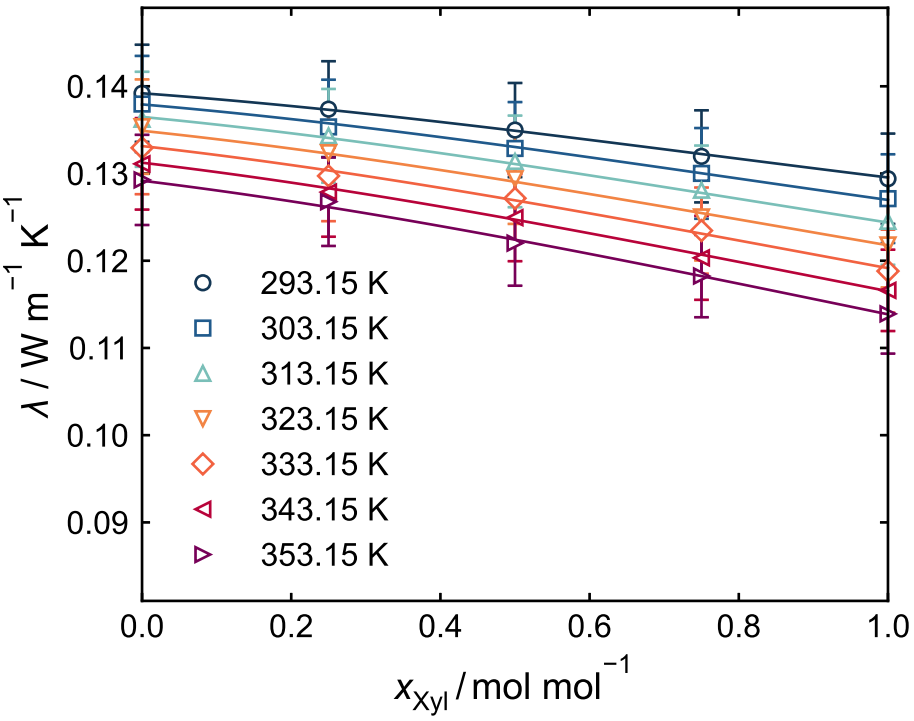

Figure 3: Thermal conductivity λ of mixtures of EHA and *p*-xylene at 101.3 kPa and different temperatures. Symbols are experimental results. Error bars indicate the combined expanded uncertainty. Lines are empirical correlations, cf. Eqs. (2) – (4), with parameters listed in Tables 2 and 3.

coefficient $Đ$ over the entire composition range:

$$Đ = (Đ^{\infty}_{\mathrm{EHA,Xyl}})^{x_{\mathrm{EHA}}} (Đ^{\infty}_{\mathrm{Xyl,EHA}})^{x_{\mathrm{Xyl}}} \tag{16}$$

The Fickian mutual diffusion coefficient D was then calculated using the Maxwell-Stefan mutual diffusion coefficient and the thermodynamic factor Γ:

$$D = Đ\Gamma, \tag{17}$$

where Γ is

$$\Gamma = 1 + x_{\mathrm{EHA}} \frac{\partial \ln \gamma_{\mathrm{EHA}}}{\partial x_{\mathrm{EHA}}} = 1 + x_{\mathrm{Xyl}} \frac{\partial \ln \gamma_{\mathrm{Xyl}}}{\partial x_{\mathrm{Xyl}}} \tag{18}$$

in the present binary system. Therein, the activity coefficients γ_i and their derivatives were

Table 10: Results of the isobaric heat capacity measurements[a]

	c_p / J mol^{-1} K^{-1}				
	x_{Xyl} / mol mol^{-1}				
T / K	0[b]	0.25	0.5	0.75	1
293.15	256	239	221	203	186
303.15	261	242	224	206	189
313.15	265	247	228	209	190
323.15	271	251	231	211	192
333.15	274	253	234	214	194
343.15	278	257	237	216	196
353.15	283	263	239	219	198

[a] Isobaric heat capacity c_p, liquid mole fraction x_{Xyl}, and temperature T at $p =$ 101.3 kPa. The combined expanded relative uncertainty of the isobaric heat capacity is $U_{\mathrm{rel}}(c_p) = 0.06$ ($k = 2$) and the other combined expanded uncertainties are $U(x_{\mathrm{Xyl}}) = 0.001$ mol mol^{-1} ($k = 2$), $u(p) = 3$ kPa, and $u(T) = 0.1$ K.
[b] Repeated from Ref. 14 for the reader's convenience

Table 11: Results of the self-diffusion coefficient measurements for EHA[a]

	D_{EHA} / 10^{-9} m^2 s^{-1} ($U(D_{\mathrm{EHA}})$ / 10^{-9} m^2 s^{-1})					
	x_{Xyl} / mol mol^{-1}					
T / K	0[b]	0.02	0.25	0.50	0.75	0.95
298.15	0.127 (0.001)	0.136 (0.001)	0.246 (0.002)	0.429 (0.002)	0.664 (0.003)	0.970 (0.007)
313.15	0.214 (0.001)	0.229 (0.002)	0.372 (0.002)	0.596 (0.004)	0.887 (0.004)	1.178 (0.015)
333.15	0.375 (0.001)	0.395 (0.002)	0.569 (0.004)	0.835 (0.004)	1.191 (0.011)	1.590 (0.016)

[a] Self-diffusion coefficient D_{EHA}, liquid mole fraction x_{Xyl}, and temperature T at $p = 101.3$ kPa. The combined expanded uncertainties of the self-diffusion coefficient $U(D_{\mathrm{EHA}})$ ($k = 2$) are given in the table and $U(x_{\mathrm{Xyl}}) = 0.001$ mol mol^{-1} ($k = 2$), $u(p) = 3$ kPa, and $u(T) = 0.1$ K.
[b] Repeated from Ref. 14 for the reader's convenience

obtained from the NRTL model fitted to the VLE data (see Eqs. (12) – (13) and Table 6).

Figure 7 shows the Lewis number of mixtures of EHA and *p*-xylene as a function of composition at different temperatures. The Lewis number decreases with increasing tem-

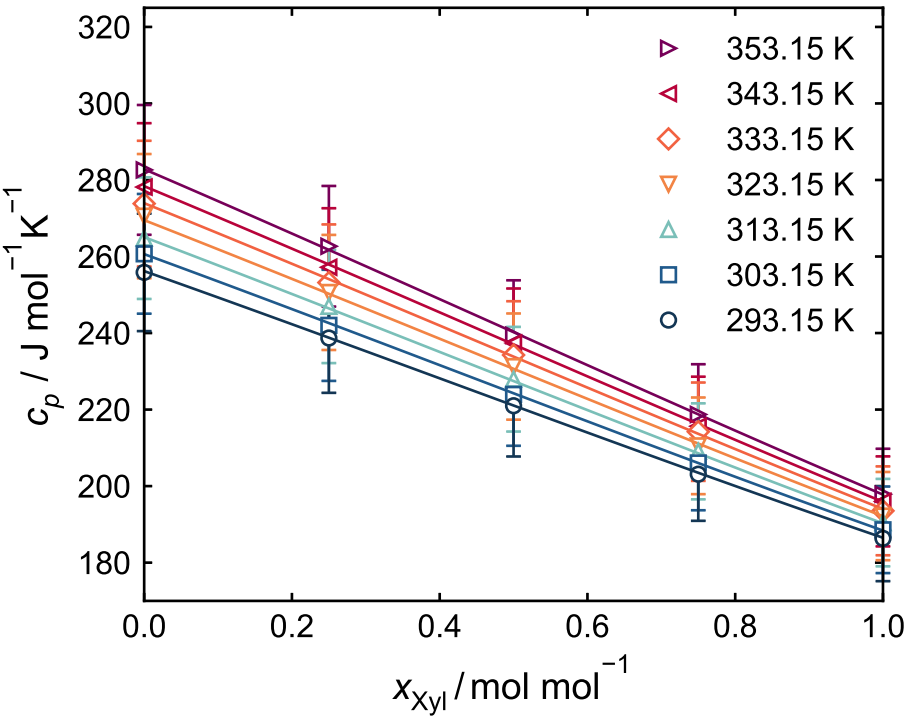

Figure 4: Isobaric heat capacity c_p of mixtures of EHA and *p*-xylene at 101.3 kPa and different temperatures. Symbols are experimental results. Error bars indicate the combined expanded uncertainty. Lines are empirical correlations, cf. Eqs. (2) – (4), with parameters listed in Tables 2 and 3.

Table 12: Results of the self-diffusion coefficient measurements for *p*-xylene[a]

	D_{Xyl} / 10^{-9} m^2 s^{-1} ($U(D_{Xyl})$ / 10^{-9} m^2 s^{-1})					
	x_{Xyl} / mol mol^{-1}					
T / K	0.02	0.25	0.50	0.75	0.95	1
298.15	0.305 (0.022)	0.676 (0.006)	1.069 (0.004)	1.522 (0.003)	2.002 (0.003)	2.109 (0.004)
313.15	0.502 (0.024)	0.956 (0.013)	1.435 (0.004)	1.964 (0.005)	2.467 (0.004)	2.602 (0.005)
333.15	0.773 (0.044)	1.313 (0.040)	1.897 (0.014)	2.561 (0.013)	3.188 (0.014)	3.354 (0.025)

[a] Self-diffusion coefficient D_{Xyl}, liquid mole fraction x_{Xyl}, and temperature T at p = 101.3 kPa. The combined expanded uncertainties of the self-diffusion coefficient $U(D_{Xyl})$ (k = 2) are given in the table and $U(x_{Xyl})$ = 0.001 mol mol^{-1} (k = 2), $u(p)$ = 3 kPa, and $u(T)$ = 0.1 K.

perature. It is highest for high concentrations of EHA, reaches a local minimum at around x_{Xyl} = 0.8 mol mol^{-1}, and increases slightly again for higher *p*-xylene mole fractions. The Lewis number is overall very high with values between 20 and almost 400, indicating that the heat transport is much faster than the diffusive mass transport in mixtures of EHA and

Table 13: Results of the isobaric VLE measurements[a]

p / kPa	T / K	x_{Xyl} / mol mol^{-1}	y_{Xyl} / mol mol^{-1}
10	404.9	0.063	0.701
	382.1	0.166	0.932
	373.2	0.236	0.966
	367.2	0.284	0.978
	362.2	0.356	0.984
	346.4	0.720	0.996
	344.3	0.796	0.995
	342.4	0.901	0.995
20	409.9	0.136	0.821
	395.9	0.189	0.903
	394.1	0.209	0.916
	391.5	0.239	0.933
	385.1	0.314	0.970
	377.1	0.425	0.981
	374.1	0.498	0.985
	370.1	0.579	0.989
	369.9	0.563	0.984
	369.5	0.546	0.983
	366.8	0.987	0.987
	365.3	0.704	0.990
	365.3	0.702	0.990
	361.3	0.825	0.993
	359.3	0.959	0.994

[a] Pressure p, temperature T, liquid phase mole fraction x_{Xyl}, and vapor phase mole fraction y_{Xyl}. The standard uncertainties are $u(p) = 0.1$ kPa, $u(T) = 0.1$ K, $u(x_{\mathrm{Xyl}}) = u(y_{\mathrm{Xyl}}) = 0.01$ mol mol^{-1}

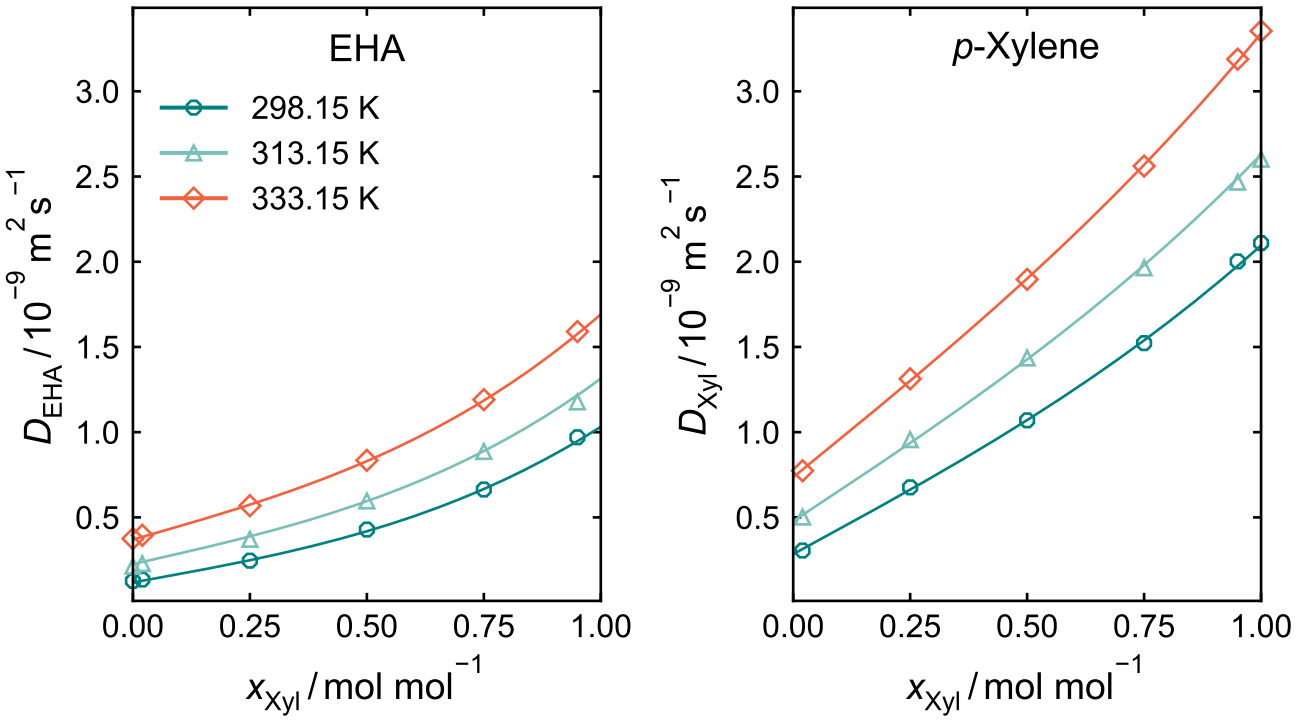

Figure 5: Self-diffusion coefficients of EHA D_{EHA} (left) and *p*-xylene D_{Xyl} (right) in mixtures of EHA and *p*-xylene at 101.3 kPa and different temperatures. Symbols are experimental results. Experimental uncertainties are within symbol size. Lines are empirical correlations, cf. Eq. (9), with parameters listed in Table 4.

p-xylene.

Due to the relatively slow mass transport and the wide-boiling VLE, EHA will tend to accumulate at the droplet surface during droplet evaporation. If the temperature continues to rise throughout the droplet, as promoted by the comparatively fast heat transfer, superheating can occur in the droplet interior, as shown for mixtures of TTIP and *p*-xylene in Ref. 29. Eventually, this superheating can lead to droplet micro-explosions. This agrees with the fact that micro-explosions have been observed in single droplet combustion experiments with mixtures of EHA and *p*-xylene.[8]

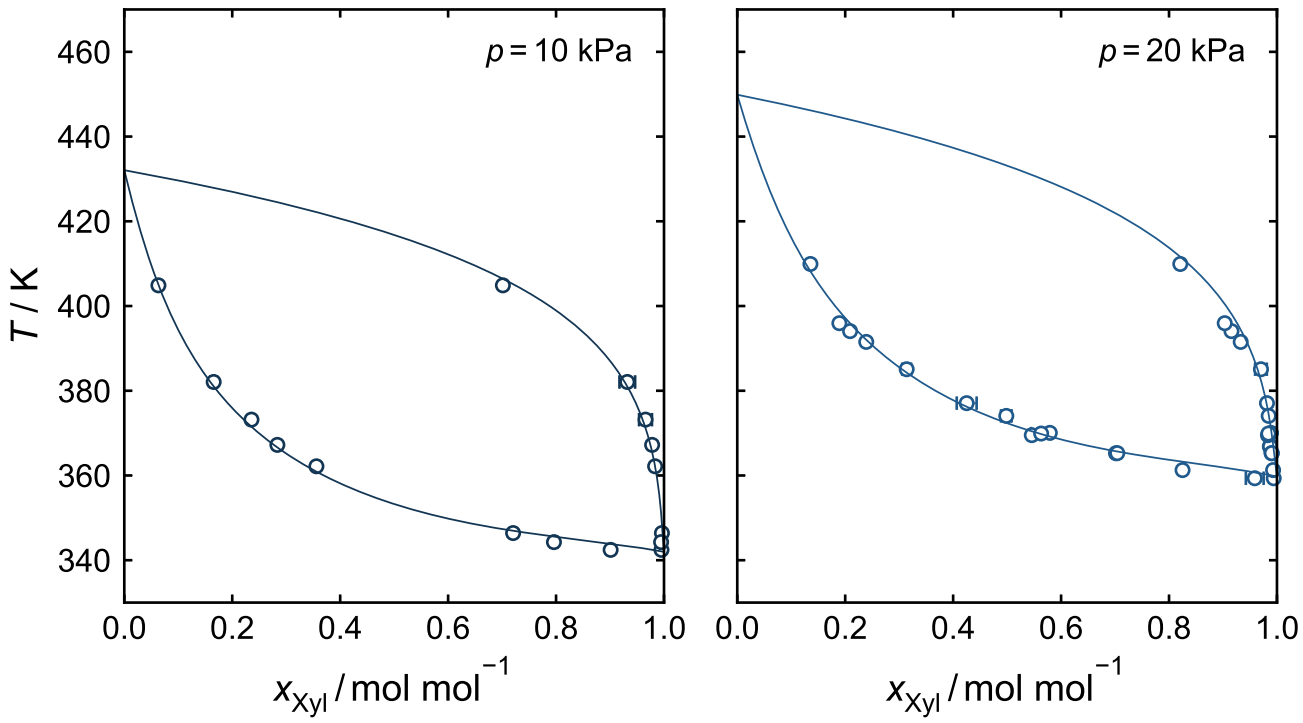

Figure 6: VLE of mixtures of EHA and *p*-xylene. Symbols are experimental results. Error bars indicate the experimental standard uncertainty. Lines show modeling results using the extended Raoult's law and the NRTL model for the activity coefficients, cf. Eqs. (10) – (13), with parameters listed in Tables 5 and 6.

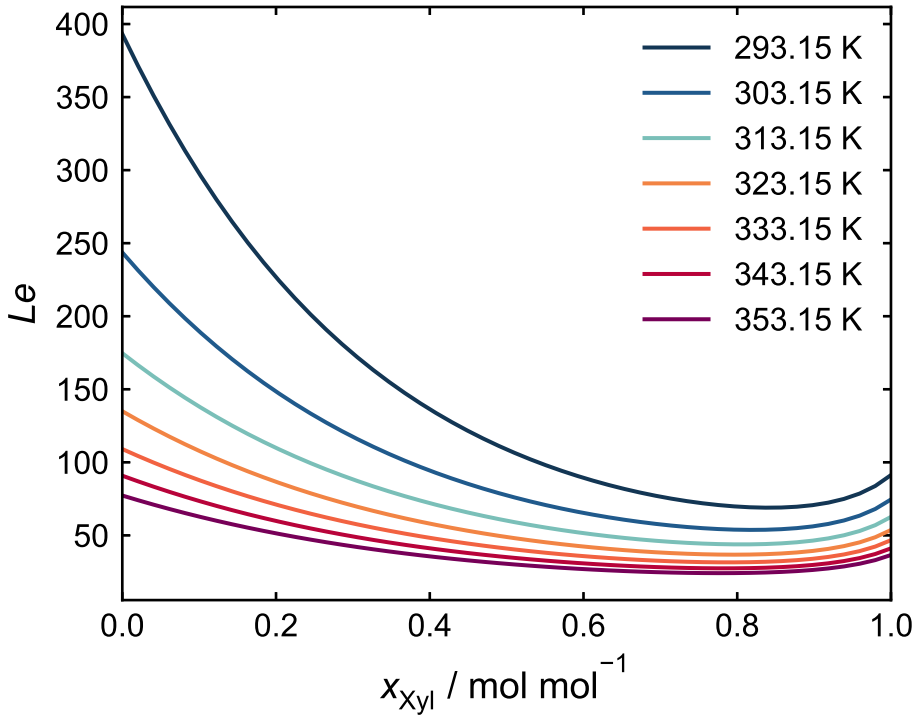

Figure 7: Lewis number Le of mixtures of EHA and p-xylene at 101.3 kPa and different temperatures.

Conclusions

In this work, the thermophysical properties of mixtures of EHA an *p*-xylene, namely the density, the viscosity, the thermal conductivity, and the isobaric heat capacity, as well as the self-diffusion coefficients and VLE, were investigated over the entire composition range at temperatures between 293.15 and 353.15 K. As expected, the density, the viscosity, and the thermal conductivity decrease with increasing temperature, while the isobaric heat capacity and the self-diffusion increase with increasing temperature. All properties, except the molar volume and the isobaric heat capacity, show significant deviations from ideal mixing behavior. Namely, especially the viscosity, the thermal conductivity, and the self-diffusion coefficients show strong deviations from linear dependence on the molar composition.

The VLE is wide-boiling and zeotropic. Together with the high Lewis numbers, this can lead to superheating and micro-explosions during the evaporation of droplets consisting of EHA and *p*-xylene, e.g., during spray flame synthesis. The property correlations provided in this work enable the use of the data in models and simulations of spray flame synthesis to deepen process understanding and improve product quality.

Appendix

Figure A1 shows the experimental results for the molar volume together with the correlation results. The molar volume decreases with decreasing temperature and increasing *p*-xylene mole fraction. The almost perfectly linear dependence on the molar composition indicates an approximately ideal behavior of this property.

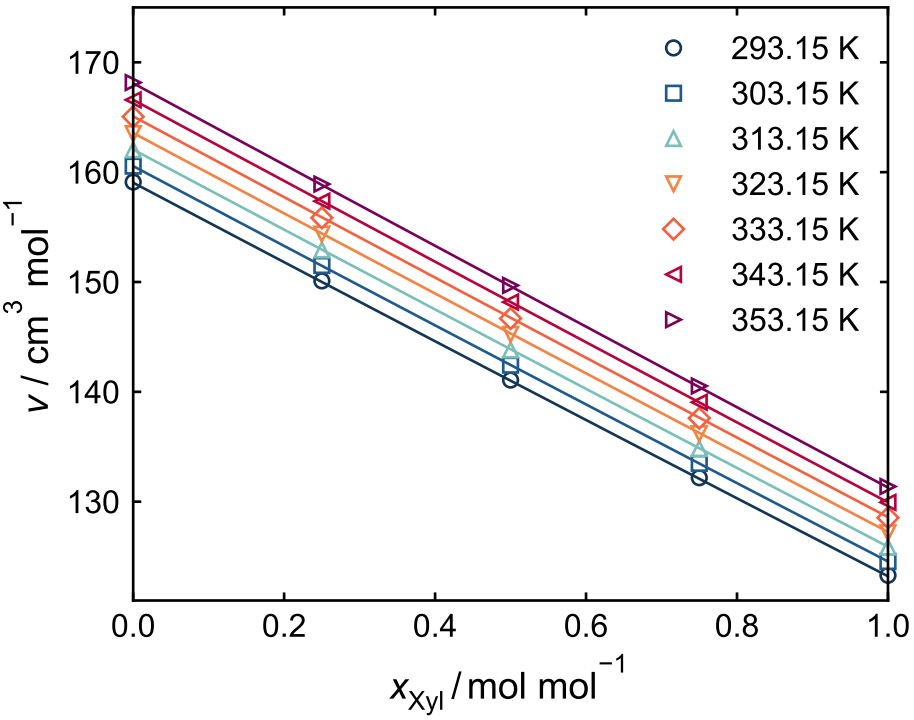

Figure A1: Molar volume v of mixtures of EHA and *p*-xylene at 101.3 kPa and different temperatures. Symbols are experimental results. Experimental uncertainties are within symbol size. Lines are empirical correlations, cf. Eqs. (2) – (6), with parameters listed in Tables 2 and 3.

Acknowledgement

This work was supported by the German Research Foundation (DFG) within the priority program SPP 1980 SPRAYSYN under the grants HA 1993/18-2 and KO 5844/2-2.

The authors thank Felix Bartzack, Hanna Kasten, Tobias Laufer, and Xueqi Zhang for their support in carrying out the experimental work.

The authors respectfully acknowledge Maria Eugénia Macedo's contributions to the fields of applied thermodynamics and separation technology.

References

(1) Schimmoeller, B.; Jiang, Y.; Pratsinis, S. E.; Baiker, A. Structure of flame-made vanadia/silica and catalytic behavior in the oxidative dehydrogenation of propane. *Journal of Catalysis* **2010**, *274*, 64–75.

(2) Strobel, R.; Pratsinis, S. E. Effect of solvent composition on oxide morphology during flame spray pyrolysis of metal nitrates. *Physical Chemistry Chemical Physics* **2011**, *13*, 9246–9252.

(3) Boningari, T.; Koirala, R.; Smirniotis, P. G. Low-temperature catalytic reduction of NO by NH_3 over vanadia-based nanoparticles prepared by flame-assisted spray pyrolysis: Influence of various supports. *Applied Catalysis B: Environmental* **2013**, *140-141*, 289–298.

(4) Waser, O.; Hess, M.; Güntner, A.; Novák, P.; Pratsinis, S. E. Size controlled CuO nanoparticles for Li-ion batteries. *Journal of Power Sources* **2013**, *241*, 415–422.

(5) Rosebrock, C. D.; Wriedt, T.; Mädler, L.; Wegner, K. The role of microexplosions in flame spray synthesis for homogeneous nanopowders from low-cost metal precursors. *AIChE Journal* **2016**, *62*, 381–391.

(6) Waser, O.; Brenner, O.; Groehn, A. J.; Pratsinis, S. E. Process Design for Size-Controlled Flame Spray Synthesis of $Li_4Ti_5O_{12}$ and Electrochemical Performance. *Chemical and Process Engineering* **2017**, *38*, 51–66.

(7) Meierhofer, F.; Li, H.; Gockeln, M.; Kun, R.; Grieb, T.; Rosenauer, A.; Fritsching, U.; Kiefer, J.; Birkenstock, J.; Mädler, L.; Pokhrel, S. Screening precursor-solvent combinations for $Li_4Ti_5O_{12}$ energy storage material using flame spray pyrolysis. *ACS Applied Materials and Interfaces* **2017**, *9*, 37760–37777.

(8) Rosebrock, C. D.; Riefler, N.; Wriedt, T.; Mädler, L.; Tse, S. D. Disruptive burning of precursor/solvent droplets in flame-spray synthesis of nanoparticles. *AIChE Journal* **2013**, *59*, 4553–4566.

(9) Li, H.; Rosebrock, C. D.; Wu, Y.; Wriedt, T.; Mädler, L. Single droplet combustion of precursor/solvent solutions for nanoparticle production: Optical diagnostics on single isolated burning droplets with micro-explosions. *Proceedings of the Combustion Institute* **2019**, *37*, 1203–1211.

(10) Li, H.; Pokhrel, S.; Schowalter, M.; Rosenauer, A.; Kiefer, J.; Mädler, L. The gas-phase formation of tin dioxide nanoparticles in single droplet combustion and flame spray pyrolysis. *Combustion and Flame* **2020**, *215*, 389–400.

(11) Ren, Y.; Cai, J.; Pitsch, H. Theoretical single-droplet model for particle formation in flame spray pyrolysis. *Energy and Fuels* **2021**, *35*, 1750–1759.

(12) Keller, A.; Wlokas, I.; Kohns, M.; Hasse, H. Thermophysical properties of mixtures of titanium(IV) isopropoxide (TTIP) and *p*-xylene. *Journal of Chemical and Engineering Data* **2020**, *65*, 869–876.

(13) Garrido, N. M.; Jorge, M.; Queimada, A. J.; Gomes, J. R. B.; Economou, I. G.; Macedo, E. A. Predicting hydration Gibbs energies of alkyl-aromatics using molecular simulation: a comparison of current force fields and the development of a new

parameter set for accurate solvation data. *Physical Chemistry Chemical Physics* **2011**, *13*, 17384.

(14) Kunstmann, B.; Kohns, M.; Hasse, H. Thermophysical Properties of Mixtures of 2-Ethylhexanoic Acid and Ethanol. *Journal of Chemical and Engineering Data* **2023**, *68*, 330–338.

(15) Keller, A.; Wlokas, I.; Kohns, M.; Hasse, H. Thermophysical Properties of Solutions of Iron(III) Nitrate Nonahydrate in Mixtures of 1-Propanol and Water. *Journal of Chemical and Engineering Data* **2020**, *65*, 5413–5420.

(16) Keller, A.; Wlokas, I.; Kohns, M.; Hasse, H. Thermophysical properties of solutions of iron(III) nitrate-nonahydrate in mixtures of ethanol and water. *Journal of Chemical and Engineering Data* **2020**, *65*, 3519–3527.

(17) Bellaire, D.; Kiepfer, H.; Münnemann, K.; Hasse, H. PFG-NMR and MD simulation study of self-diffusion coefficients of binary and ternary mixtures containing cyclohexane, ethanol, acetone, and toluene. *Journal of Chemical and Engineering Data* **2020**, *65*, 793–803.

(18) Bellaire, D.; Großmann, O.; Münnemann, K.; Hasse, H. Diffusion coefficients at infinite dilution of carbon dioxide and methane in water, ethanol, cyclohexane, toluene, methanol, and acetone: A PFG-NMR and MD simulation study. *The Journal of Chemical Thermodynamics* **2022**, *166*, 106691.

(19) Stejskal, E. O.; Tanner, J. E. Spin diffusion measurements: Spin echoes in the presence of a time-dependent field gradient. *The Journal of Chemical Physics* **1965**, *42*, 288–292.

(20) Hasse, H. Dampf-Flüssigkeits-Gleichgewichte, Enthalpien und Reaktionskinetik in formaldehydhaltigen Mischungen. PhD thesis, TU Kaiserslautern, 1990.

(21) Hasse, H.; Hahnenstein, I.; Maurer, G. Revised vapor-liquid equilibrium model for multicomponent formaldehyde mixtures. *AIChE Journal* **1990**, *36*, 1807–1814.

(22) Dyga, M.; Keller, A.; Hasse, H. 13 C-NMR Spectroscopic Study of the Kinetics of Formaldehyde Oligomerization Reactions in the System (Formaldehyde + Water + Isoprenol). *Industrial and Engineering Chemistry Research* **2022**, *61*, 224–235.

(23) Keller, A.; Wlokas, I.; Kohns, M.; Hasse, H. Thermophysical properties of mixtures of titanium(IV) isopropoxide (TTIP) and 2-propanol (iPOH). *Journal of Chemical and Engineering Data* **2021**, *66*, 1296–1304.

(24) Jouyban, A.; Khoubnasabjafari, M.; Vaez-Gharamaleki, Z.; Fekari, Z.; Acree, W. E. Calculation of the Viscosity of Binary Liquids at Various Temperatures Using Jouyban–Acree Model. *Chemical and Pharmaceutical Bulletin* **2005**, *53*, 519–523.

(25) Steele, W. V.; Chirico, R. D.; Knipmeyer, S. E.; Nguyen, A. Vapor pressure, heat capacity, and density along the saturation line, measurements for cyclohexanol, 2-cyclohexen-1-one, 1,2-dichloropropane, 1,4-di-tert-butylbenzene, (±)-2-ethylhexanoic Acid, 2-(methylamino)ethanol, perfluoro-n-heptane, and sulfolan. *Journal of Chemical and Engineering Data* **1997**, *42*, 1021–1036.

(26) Fendu, E. M.; Nicolae, M.; Oprea, F. Vapour-liquid equilibrium for tripropylene glycol + aromatic hydrocarbons binary systems: Measurements and modelling. *Fluid Phase Equilibria* **2016**, *425*, 188–195.

(27) Renon, H.; Prausnitz, J. M. Local compositions in thermodynamic excess functions for liquid mixtures. *AIChE Journal* **1968**, *14*, 135–144.

(28) Mengarelli, A. C.; Brignole, E. A.; Bottini, S. B. Activity coefficients of associating mixtures by group contribution. *Fluid Phase Equilibria* **1999**, *163*, 195–207.

(29) Kunstmann, B.; Wlokas, I.; Kohns, M.; Hasse, H. Simulation study of superheating in evaporating droplets of (TTIP + *p*-xylene) in spray flame synthesis. *Applications in Energy and Combustion Science* **2023**, *15*, 100156.

(30) Law, C. K. Internal boiling and superheating in vaporizing multicomponent droplets. *AIChE Journal* **1978**, *24*, 626–632.

(31) Vignes, A. Diffusion in Binary Solutions: Variation of Diffusion Coefficient with Composition. *Industrial and Engineering Chemistry Fundamentals* **1966**, *5*, 189–199.